Volume 8, Number 1, 2015. pp. 39-47

Jordan Journal of Physics

ARTICLE

Reflection of Polarized Light at Quasi-Index-Matched Dielectric-Conductor Interfaces

R. M. A. Azzam

Department of Electrical Engineering, University of New Orleans, New Orleans, Louisiana 70148, USA.

Received on: 20/1/2015; Accepted on: 7/7/2015

Abstract: Quasi-index-matched (QIM) dielectric-conductor interfaces are characterized by a unit-magnitude complex relative dielectric function, $\varepsilon = \exp(-j\theta), 0 \le \theta \le \pi,$ and exhibit minimum reflectance at normal incidence. Their reflection properties are analyzed in detail as functions of the incident linear polarization (p or s), angle of incidence ϕ and θ. Complex-plane trajectories of the Fresnel reflection coefficients $r_p(\phi)$, $r_s(\phi)$ and their ratio $\rho(\phi) = r_p / r_s = \tan\psi \exp(j\Delta)$ as ϕ increases from 0 to 90° are presented at discrete values of θ. Absolute values and phase angles of r_p, r_s and ρ are also plotted as functions of ϕ. Finally, the pseudo-Brewster angle of minimum $|r_p|$, the second-Brewster angle of minimum $|\rho|$, the principal angle at which $\Delta = \pi/2$ and the special angle $(\phi = \sin^{-1}\sqrt{0.5\sec\theta})$ at which $\delta_p = \arg(r_p) = \pm\pi$ of QIM interfaces are determined as functions of θ.

Keywords: Physical optics; Reflection; Interfaces; Polarization; Dielectric function; Ellipsometry.
PACS: 42. Optics.

1. Introduction

The reflectance of monochromatic light at normal incidence by the plane boundary between a transparent medium of incidence with real dielectric function ε_0 and an absorbing medium of refraction with complex dielectric function ε_1 is minimized when $\varepsilon_0 = |\varepsilon_1|$. The complex relative dielectric function $\varepsilon = \varepsilon_1 / \varepsilon_0$ of such quasi-index-matched (QIM) interfaces [1] has unit magnitude and is expressed in polar form as:

$$\varepsilon = \exp(-j\theta), 0 \le \theta \le \pi. \tag{1}$$

The range of θ in Eq. (1) is consistent with the $\exp(-j\omega t)$ time dependence (j is the pure imaginary number and ω is the angular frequency) and the Nebraska-Muller conventions [2]. Specific examples of interfaces that satisfy the QIM condition in different spectral regions are given in Appendix A.

For a given ε, the complex-amplitude Fresnel reflection coefficients of p- and s-polarized light at an oblique angle of incidence ϕ are given by [3, 4]:

Corresponding Author: R. M. A. Azzam **Email**: razzam@uno.edu

$$r_p = \frac{\varepsilon\cos\phi - (\varepsilon - \sin^2\phi)^{1/2}}{\varepsilon\cos\phi + (\varepsilon - \sin^2\phi)^{1/2}}, \quad (2)$$

$$r_s = \frac{\cos\phi - (\varepsilon - \sin^2\phi)^{1/2}}{\cos\phi + (\varepsilon - \sin^2\phi)^{1/2}}. \quad (3)$$

At normal incidence $(\phi = 0)$, the reflection coefficients r_p, r_s of QIM interfaces with unit-magnitude relative dielectric function [Eq. (1)] reduce to:

$$r_p = -j\tan(\theta/4), r_s = +j\tan(\theta/4). \quad (4)$$

From Eqs. (4), it is apparent that the reflection p- and s-polarized light at normal incidence by QIM interfaces is accompanied by quarter-wave $(\mp\pi/2)$ phase shifts and that the associated amplitude reflectances are equal to the tangent of one-fourth the angle θ of complex ε.

In this study, the complex reflection coefficients r_p, r_s, and ellipsometric function [3, 5],

$$\left.\begin{aligned}\rho &= r_p / r_s = \tan\psi \exp(j\Delta)\\ &= \frac{\sin\phi\tan\phi - (\varepsilon - \sin^2\phi)^{1/2}}{\sin\phi\tan\phi + (\varepsilon - \sin^2\phi)^{1/2}},\end{aligned}\right\} \quad (5)$$

of QIM dielectric-conductor interfaces are considered in detail as functions of both ϕ and θ.

In Section 2, complex-plane trajectories of r_p and r_s as the angle of incidence ϕ increases from $\phi = 0$ [initial values given by Eqs. (4)] to $\phi = 90^\circ$ [$r_p = r_s = -1$] are presented at discrete values of θ in the range $0 \le \theta \le 180^\circ$. Amplitude reflectances $|r_p|$, $|r_s|$ and phase shifts $\delta_p = \arg(r_p)$, $\delta_s = \arg(r_s)$ are also plotted as functions of ϕ at the same discrete values of θ.

In Section 3, trajectories of $\rho(\phi)$, $0 \le \phi \le 90^\circ$, in the complex plane and graphs of the ellipsometric parameters $\tan\psi$ and Δ *versus* ϕ at constant values of θ are presented.

In Section 4, the pseudo-Brewster angle of minimum reflectance for incident p-polarized light [6 - 9], the principal angle at which the differential reflection phase shift $\Delta = \pi/2$ [7, 10], the second-Brewster angle of minimum reflectance ratio $|\rho|$ [11] and the special angle at which the reflection phase shift of p-polarized light $\delta_p = \pm\pi$ [12] are all determined as functions of θ for all QIM dielectric-conductor interfaces.

Section 5 gives a brief summary of this work.

2. Reflection Coefficients of *p*- and *s*-Polarized Light at QIM Dielectric-Conductor Interfaces

Fig. 1 shows the complex-plane trajectories of $r_p(\phi)$ as ϕ increases from 0 [initial values $r_p(0)$ along the negative imaginary axis *ON* given by Eqs. (4)] to 90° ($r_p = -1$ at point *G*) for QIM dielectric-conductor interfaces with $\theta = 0.1^\circ$ and $\theta = 10^\circ$ to 180° in equal steps of 10°.

Note that $\theta = 0$ represents a vanishing optical interface with $\varepsilon = 1$, so that $r_p = r_s = 0$ at all angles of incidence and the corresponding trajectory collapses to a single point at the origin *O*. For $\theta = 180^\circ$ and $\varepsilon = -1$ (an ideal dielectric-plasma interface), total reflection takes place $|r_p| = |r_s| = 1$ at all incidence angles, and the corresponding locus of $r_p(\phi)$ becomes the arc *NG* of the unit circle in the third quadrant of the complex plane. The ϕ- dependent phase shift along this unit-circle arc is derived from Eq. (2) as:

$$\delta_p(\phi) = -2\tan^{-1}[(1+\sin^2\phi)^{1/2}/\cos\phi]. \quad (6)$$

The top and bottom parts of Fig. 2 show the amplitude and phase plots $|r_p|(\phi)$ and $\delta_p(\phi)$, respectively, for $\theta = 0.1^\circ$ and $\theta = 10^\circ$ to 180° in equal steps of 10°. The pseudo-Brewster angle ϕ_{pB} of minimum $|r_p|$ is < 45° for all values of θ, as is discussed further in Section 4. The angles of incidence at which $\delta_p = \pm 180^\circ$ (located at the vertical transitions in the $\delta_p - vs - \phi$ curves) are also determined in Section 4.

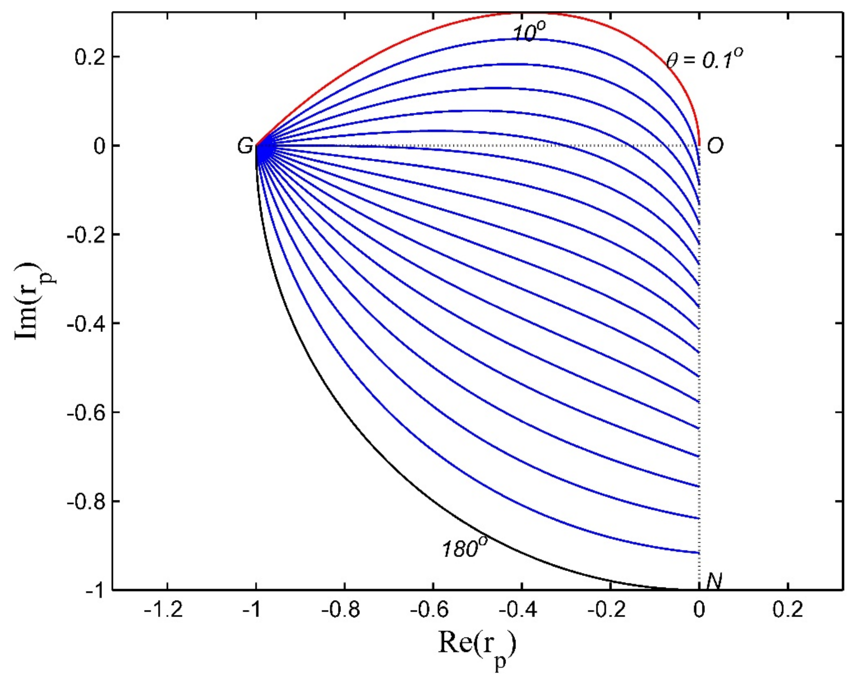

FIG. 1. Complex-plane trajectories of $r_p(\phi)$ as ϕ increases from 0 [initial values $r_p(0)$ along the negative imaginary axis *ON* are given by Eqs. (4)] to 90° ($r_p = -1$ at point *G*) of QIM dielectric-conductor interfaces with $\theta = 0.1^\circ$ and $\theta = 10^\circ$ to 180° in equal steps of 10°.

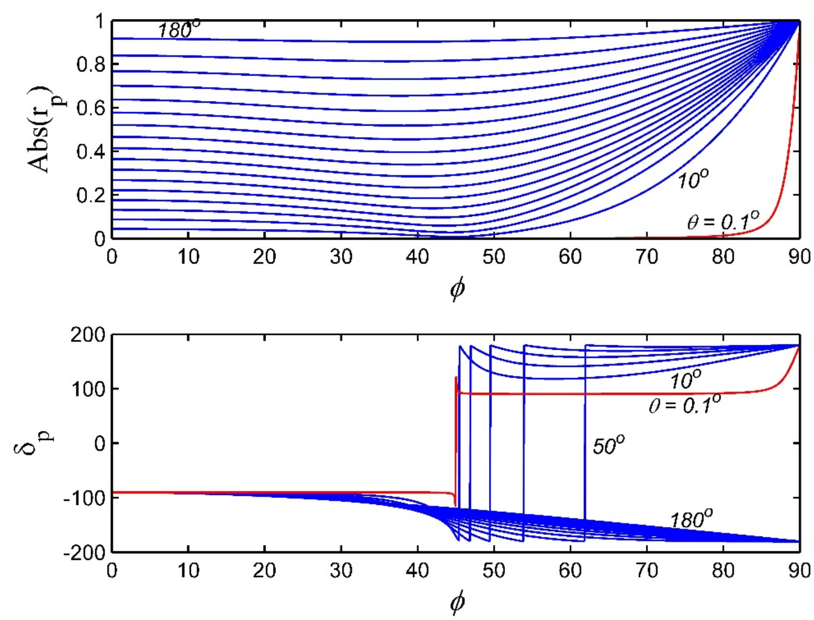

FIG. 2. Amplitude reflectance $|r_p|(\phi)$, top, and phase shift $\delta_p(\phi)$, bottom, as functions of incidence angle ϕ for QIM interfaces with $\theta = 0.1^\circ$ and $\theta = 10^\circ$ to 180° in equal steps of 10°.

Fig. 3 shows the complex-plane trajectories of $r_s(\phi)$ as ϕ increases from 0 to 90°, with initial values $r_s(0)$ located on the positive imaginary axis *ON* [given by Eqs. (4)] and the same θ values used in Fig. 1. In the limiting case of $\theta = 180^\circ$, the locus of $r_s(\phi)$ is the arc *NG* of the unit circle in the second quadrant of the complex plane. The associated ϕ- dependent phase shift $\delta_s(\phi)$ equals the negative of $\delta_p(\phi)$ given by Eq. (6).

The amplitude reflectance of s-polarized light $|r_s|(\phi)$ and associated reflection phase shift $\delta_s(\phi)$ are plotted in the top and bottom parts of Fig. 4, respectively. Both $|r_s|$ and δ_s increase monotonically with ϕ from normal to grazing incidence.

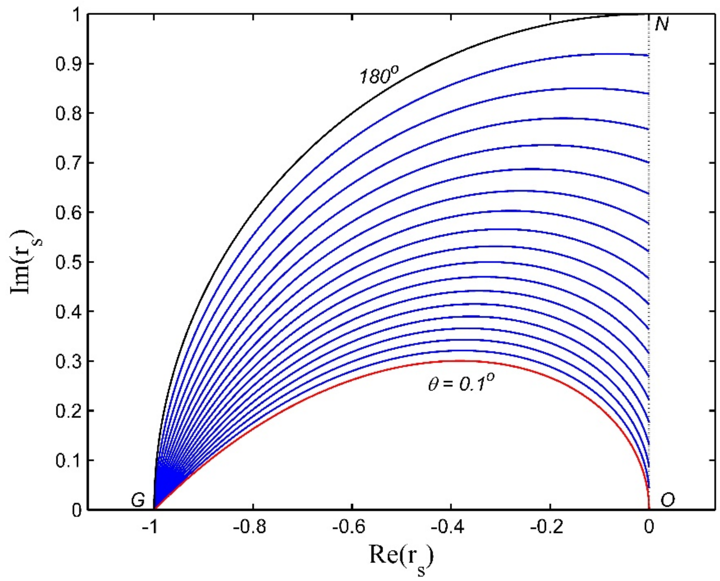

FIG. 3. Complex-plane trajectories of $r_s(\phi)$ as ϕ increases from 0 [initial values $r_s(0)$ along the positive imaginary axis *ON* are given by Eqs. (4)] to 90° ($r_s = -1$ at point *G*) of QIM dielectric-conductor interfaces with $\theta = 0.1^\circ$ and $\theta = 10^\circ$ to 180° in equal steps of 10°.

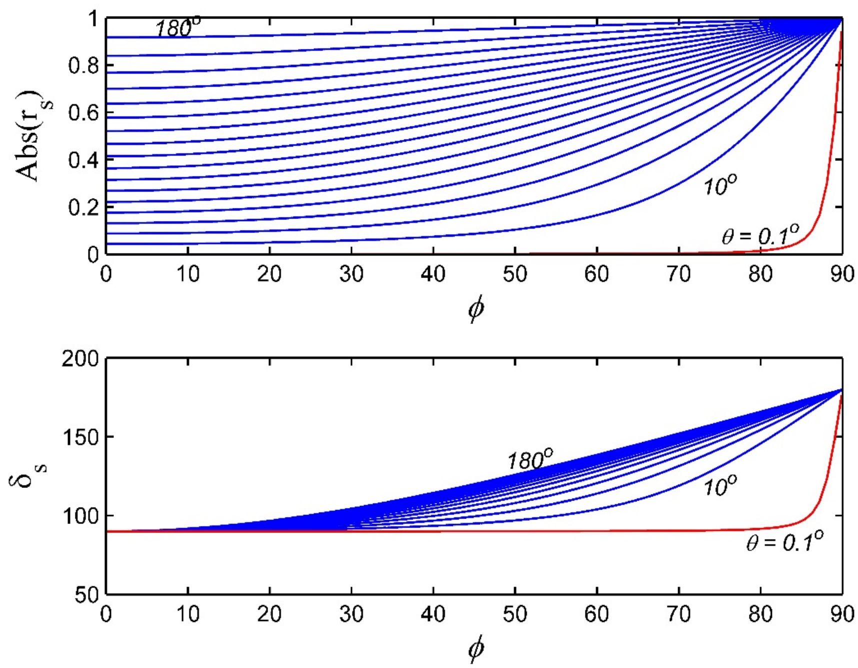

FIG. 4. Amplitude reflectance $|r_s|(\phi)$, top, and phase shift $\delta_s(\phi)$, bottom, as functions of incidence angle ϕ for QIM interfaces with $\theta = 0.1^\circ$ and $\theta = 10^\circ$ to 180° in equal steps of 10°.

3. Ellipsometric Function of QIM Dielectric-Conductor Interfaces

Fig. 5 shows trajectories of the ratio of complex reflection coefficients $\rho = r_p / r_s = \tan\psi \exp(j\Delta)$ as ϕ increases from normal to grazing incidence for QIM dielectric-conductor interfaces at the same θ values used in Figs. 1 and 3. All curves start at $\rho = -1$ when $\phi = 0$ (point *N*) and end at $\rho = +1$ when $\phi = 90^\circ$ (point *G*). The point of intersection of each curve with the imaginary axis (represented by the vertical dashed line in Fig. 5) defines a unique principal angle ϕ_{PA} at which $\Delta = 90^\circ$. Dependence of ϕ_{PA} on θ is presented in Section 4.

The top and bottom parts of Fig. 6 show $\tan\psi$ and Δ, respectively, as functions of ϕ along each one of the contours in Fig. 5. The $\Delta - vs - \phi$ curve at $\theta = 0.1^\circ$ is nearly a step function with vertical transition of Δ from 180° to 0° located at $\phi = 45^\circ$, which is the second Brewster angle at which $\tan\psi \approx 0$.

In Fig. 6, the $\Delta - vs - \phi$ curve at $\theta = 180^\circ$ is described by:

$$\left.\begin{array}{l}\Delta(\phi) = \\ 360^\circ - 4\tan^{-1}[(1+\sin^2\phi)^{1/2} / \cos\phi].\end{array}\right\} \quad (7)$$

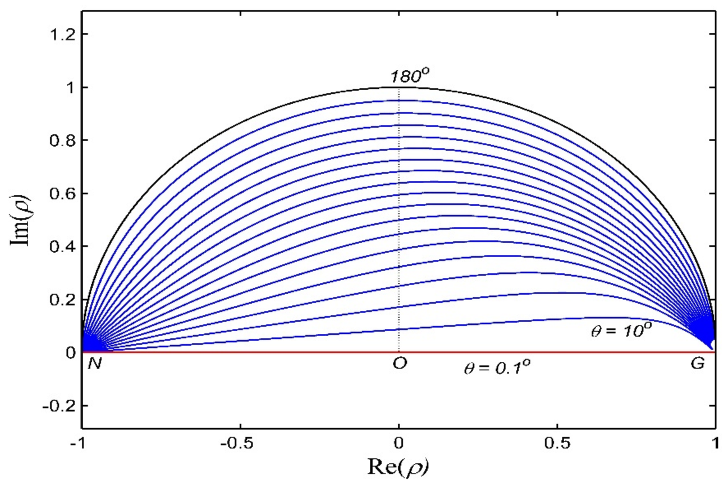

FIG. 5. Trajectories of the ellipsometric function $\rho(\phi) = r_p / r_s = \tan\psi \exp(j\Delta)$ as ϕ increases from 0 to 90° for QIM dielectric-conductor interfaces with $\theta = 0.1^\circ$ and $\theta = 10^\circ$ to 180° in equal steps of 10°.

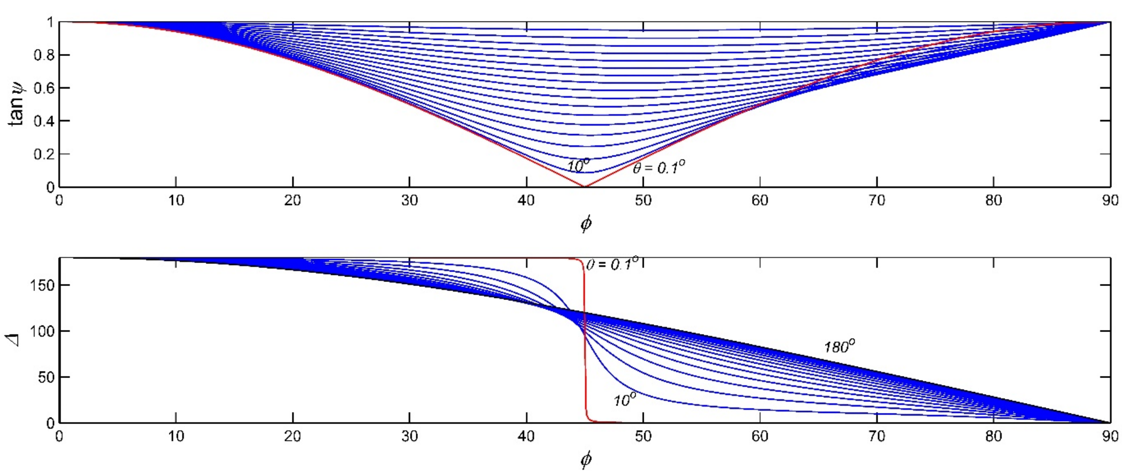

FIG. 6. Ellipsometric parameters $\tan\psi$ and Δ as functions of ϕ along each one of the contours shown in Fig. 5.

4. Special Angles of Incidence Associated with Light Reflection at QIM Dielectric-Conductor Interfaces

The pseudo-Brewster angle ϕ_{pB} of minimum $|r_p|$ of a QIM dielectric-conductor interface is determined by solving the following cubic equation [9]:

$$a_3u^3 + a_2u^2 + a_1u + a_0 = 0, \tag{8}$$

in which $u = \sin^2\phi_{pB}$ and

$$\left.\begin{aligned} a_3 &= 2\cos\theta + 2, \\ a_2 &= a_1 = -2, \\ a_0 &= 1. \end{aligned}\right\} \tag{9}$$

Likewise, the principal angle ϕ_{PA} at which $\Delta = 90^\circ$ [10] is obtained by solving another cubic equation [Eq. (8)] with $u = \sin^2\phi_{PA}$ and coefficients given by:

$$\left.\begin{aligned} a_3 &= a_1 = 2\cos\theta + 2, \\ a_2 &= 2 - 2a_1, \\ a_0 &= -1. \end{aligned}\right\} \tag{10}$$

The second-Brewster angle ϕ_{2B} of minimum $|\rho|$ of a QIM interface is determined by solving a quartic equation [11],

$$a_4u^4 + a_3u^3 + a_2u^2 + a_1u + a_0 = 0, \tag{11}$$

with $u = \sin^2\phi_{2B}$ and

$$\left.\begin{aligned} a_4 &= \tan(\theta/2) - \sin\theta, \\ a_3 &= 2\sin\theta - 0.5\tan(\theta/2), \\ a_2 &= 0.5\tan(\theta/2)[\sec^2(\theta/2) - 2\cos\theta - 8], \\ a_1 &= 0.5\tan(\theta/2)[\tan^2(\theta/2) + 5], \\ a_0 &= -0.5\tan(\theta/2)\sec^2(\theta/2). \end{aligned}\right\} \tag{12}$$

Eqs. (12) are obtained by substituting $\varepsilon = \exp(-j\theta)$ into Eqs. (15), (18), (19) and (23) of [11] and applying several trigonometric identities.

Finally, the angle at which $\delta_p = \pm\pi$ [12] (at vertical transitions shown in the bottom part of Fig. 2) is given by:

$$\phi(\delta_p = \pm\pi) = \sin^{-1}\sqrt{0.5\sec\theta}. \tag{13}$$

This angle exists only within the limited range $0 < \theta < 60^\circ$.

In Fig. 7, the four special angles of incidence ϕ_{pB}, ϕ_{2B}, ϕ_{PA} and $\phi(\delta_p = \pm\pi)$, calculated from Eqs. (8) – (13), are plotted as functions of θ. As $\theta \to 0$ (i.e., for a vanishing optical interface) all angles converge to $\phi = 45^\circ$, which is represented by the horizontal dotted line in Fig. 7. Note that $\phi_{pB} < 45^\circ$ for all QIM interfaces; the four angles diverge apart as θ increases; and $\phi_{pB} < \phi_{2B} < \phi_{PA}$ over the full range $0 < \theta < 180^\circ$; an order that holds true for all values of complex ε.

Table 1 lists ϕ_{pB}, ϕ_{2B} and ϕ_{PA} for values of θ from 0° to 180° in equal steps of 30°. The fourth angle $\phi(\delta_p = \pm\pi)$ is not included, as it is readily obtained from Eq. (13).

All calculations and figures presented in this paper are obtained using Matlab [13]. The precision of determining the angles presented in Table 1 is better than 0.01°.

5. Conclusion

Detailed analysis of the reflection of *p*- and *s*-polarized light by quasi-index-matched (QIM) dielectric-conductor interfaces of unit-magnitude relative dielectric function, $\varepsilon = \exp(-j\theta), 0 \le \theta \le \pi$, is presented. Figures 1, 3 and 5 show the complex-plane trajectories of r_p, r_s and ellipsometric function $\rho = r_p / r_s = \tan\psi\exp(j\Delta)$, respectively, as ϕ increases from 0 to 90° at discrete values of θ in the range $0 \le \theta \le 180^\circ$.

Amplitude reflectances $|r_p|$, $|r_s|$, their ratio, $|\rho| = |r_p / r_s| = \tan\psi$ and reflection phase shifts $\delta_p = \arg(r_p)$, $\delta_s = \arg(r_s)$ and $\Delta = \delta_p - \delta_s$ are shown in Figs. 2, 4 and 6, respectively, as functions of ϕ at constant values of θ.

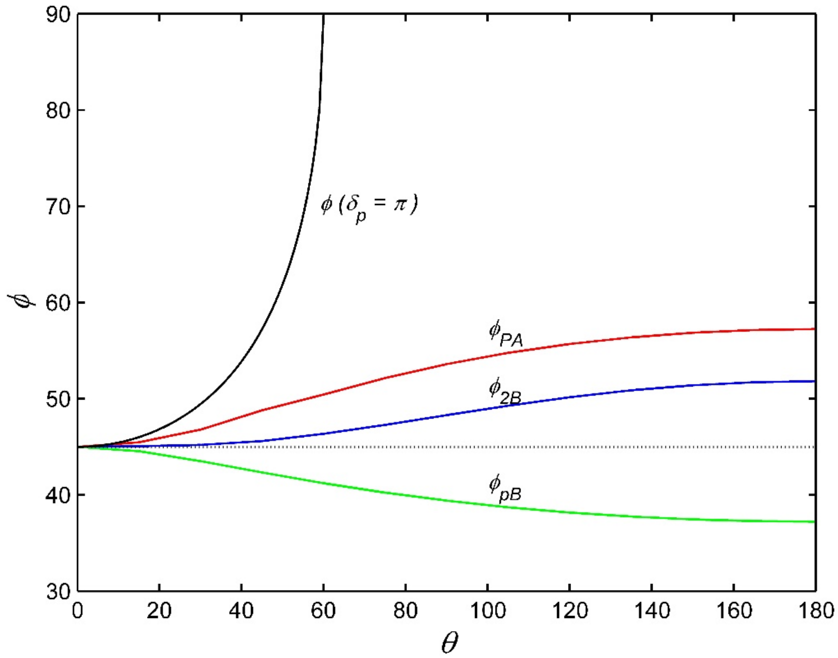

FIG. 7 Special angles of incidence $\phi_{pB}, \phi_{2B}, \phi_{PA}$ and $\phi(\delta_p = \pm\pi)$, of light reflection at QIM interfaces, calculated from Eqs. (8) - (13), are plotted as functions of θ. All angles are in degrees.

TABLE 1. Pseudo-Brewster angle ϕ_{pB} of minimum $|r_p|$, second-Brewster angle ϕ_{2B} of minimum $|\rho|$ and principal angle ϕ_{PA} at which $\Delta = \pi/2$ of QIM interfaces at selected values of θ (top row). All angles are in degrees.

$\theta \Rightarrow$	0	30	60	90	120	150	180
ϕ_{pB}	45.00	43.52	41.22	39.41	38.17	37.46	37.23
ϕ_{2B}	45.00	45.20	46.36	48.30	50.16	51.40	51.83
ϕ_{PA}	45.00	46.79	50.44	53.60	55.69	56.86	57.24

Finally, the pseudo-Brewster angle ϕ_{pB} of minimum $|r_p|$, the second-Brewster angle ϕ_{2B} of minimum $|\rho|$, the principal angle ϕ_{PA} at which $\Delta = \pi/2$ and the angle at which $\delta_p = \pm\pi$ are plotted in Fig. 7 as functions of θ for all possible QIM dielectric-conductor interfaces.

The results presented in this paper illustrate the physical optics aspects of light reflection by a unique set of interfaces with unit complex relative dielectric function. Light reflection by nearly vanishing interfaces is represented by the curves for $\theta = 0.1^\circ$ in Figs. 1 – 6. Examples of QIM interfaces in different parts of the optical spectrum are given in Appendix A.

Appendix A: Examples of QIM Interfaces

1. At the IR wavelength $\lambda = 3\mu m$, fused silica is transparent with refractive index n = 1.4193 (calculated from a dispersion relation given by Malitson [14]) and water is absorbing with complex refractive index $N = n - jk = 1.371 - j0.272$ at 25°C (from the tabular data of Hale and Querry [15]). The fused silica-water interface is characterized by $\varepsilon = (N/n)^2 = 0.9699 \exp(-j22.443^\circ)$, so that QIM is almost satisfied. It may be possible to achieve $|\varepsilon| = 1$ by changing temperature.

2. At the visible wavelength $\lambda = 500$ nm, QIM is satisfied at the interface between a transparent liquid with n = 2.060 (e.g. Cargille Optical Liquid Series EH [16]) and Au substrate with $N = 0.8472 - j1.8775$ (interpolated form data given by Lynch and Hunter [17]); for such interface $\varepsilon = 0.9998 \exp(-j131.427^\circ)$.

3. Metals have fractional optical constants $\varepsilon_r = n^2 - k^2$ and $\varepsilon_i = -2nk$ in the vacuum ultraviolet (VUV). Fig. 8 shows the real part ε_r, imaginary part, $-\varepsilon_i$ and absolute value, $abs(\varepsilon)$, of the complex dielectric function ε of Au *versus* wavelength λ in the 36 to 46 nm spectral range [17]. QIM ($abs(\varepsilon) = 1$) at the vacuum-Au interface is satisfied at point *M* at $\lambda = 39.1 nm$.

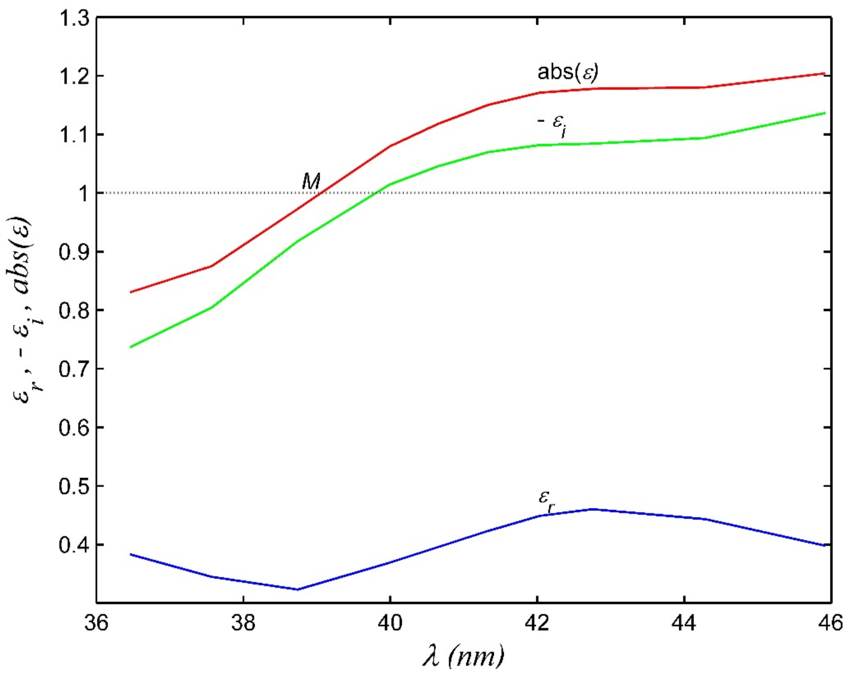

FIG. 8. Real part, ε_r, imaginary part, $-\varepsilon_i$ and absolute value, abs(ε), of the complex dielectric function of Au, $\varepsilon = (n - jk)^2$, are plotted *versus* wavelength λ in the 36-to-46 nm VUV spectral range. QIM is satisfied at point M. Optical constants *n* and *k* of Au are those of [15].

References

[1] Azzam, R.M.A. and Alsamman, A., Appl. Opt., 47 (2008) 3211.

[2] Muller, R.H., Surf. Sci., 16 (1969) 14.

[3] Azzam, R.M.A. and Bashara, N.M., "Ellipsometry and Polarized Light" (North-Holland, Amsterdam, 1987).

[4] Lekner, J., "Theory of Reflection" (Martinus Nijhoff, Dordrecht, 1987).

[5] Tompkins, H.G. and Irene, E.A., Eds., "Handbook of Ellipsometry" (William Andrew, Inc., Norwich, New York, 2005).

[6] Humphreys-Owen, S. P. F., Proc. Phys. Soc. London, 77 (1961) 949.

[7] Holl, H.B., J. Opt. Soc. Am., 57 (1967) 683.

[8] Kim, S.Y. and Vedam, K., J., Opt. Soc. Am. A, 3 (1986) 1772.

[9] Azzam, R.M.A. and Ugbo, E., Appl. Opt., 28 (1989) 5222.

[10] Azzam, R.M.A., J. Opt. Soc. Am., 71 (1981) 1523.

[11] Azzam, R.M.A., J. Opt. Soc. Am., 73 (1983) 1211.

[12] Azzam, R.M.A., J. Opt. Soc. Am., 69 (1979) 487.

[13] www.mathworks.com/products/matlab.

[14] Malitson, I.H., J. Opt. Soc. Am., 55 (1965) 1205.

[15] Hale, G.M. and Querry, M.R., Appl. Opt., 12 (1973) 555.

[16] www.cargille.com/opticalintro.shtml.

[17] Lynch, D.W. and Hunter, W.R., in "Handbook of Optical Constants of Solids" Palik, E. D., Ed. (Academic Press, New York, 1985).